Encapsulation of cationic iridium(iii) tetrazole complexes into a silica matrix: Synthesis, characterization and optical properties

Encapsulation of cationic Iridium(III) tetrazole complexes into silica matrix: synthesis, characterization and optical properties

Ilaria Zanoni, Valentina Fiorini, Marcos Rosado, Belén Ballesteros, Maria Androulidaki, Magda Blosi, Simona Ortelli, Stefano Stagni, Anna Luisa Costa. *New Journal of Chemistry* **2018**, *42*, 9635-9644

DOI: 10.1039/c8nj01514g
Publication Date (Web): May 2, 2018

Available at: http://pubs.rsc.org/en/journals/journal/nj

Encapsulation of cationic Iridium(III) tetrazole complexes into silica matrix: synthesis, characterization and optical properties

Ilaria Zanoni,[a] Valentina Fiorini,[b] Marcos Rosado,[c] Belén Ballesteros,[c] Maria Androulidaki,[d] Magda Blosi,[a] Simona Ortelli,[a] Stefano Stagni,[b] Anna Luisa Costa[a]

[a] *CNR-ISTEC-National Research Council of Italy, Institute of Science and Technology for Ceramics, Via Granarolo 64 I-48018, Faenza, RA, Italy. E mail: anna.costa@istec.cnr.it*

[b] *Department of Industrial Chemistry "Toso Montanari", University of Bologna, Viale Risorgimento 4, I-40136 Bologna, Italy.*

[c] *Catalan Institute of Nanoscience and Nanotechnology (ICN2), CSIC and BIST, Campus UAB, Bellaterra, 08193 Barcelona, Spain.*

d Microelectronics Group, IESL-FORTH, N. Plastira 100, 70013, Heraklion, Crete, Greece.

Abstract

Herein we report the easy incorporation of brightly phosphorescent cationic Iridium(III) tetrazole complexes into a silica based matrix through an easily scalable colloidal process. To this purpose, two cationic Ir(III) emitters bearing 5-aryl tetrazole ligands (R-CN_4) were selected: the blue **[F_2IrPTZ-Me]$^+$** (C^N = F_2ppy; N^N = PTZ-Me - *2-(2-methyl-2H-tetrazol-5-yl)pyridine*) and the red **[IrQTZ-Me]$^+$** (C^N = ppy; N^N = QTZ-Me - *2-(2-methyl-2H-tetrazol-5-yl)quinoline*). The cationic complexes were readily adsorbed to negatively charged silica nanoparticles and trapped in the sol-gel matrix. The *sol-to-solid* phase transfer was performed by using an innovative *spray-freeze-drying* technique, leading to the formation of phosphorescent solid micro-granules. The structural and optical characterisation of the Ir(III) complexes together with SiO_2 nanoparticles, nanosols (**Ir@SiO_2**) and powders (**Ir@SiO_2 powders**), revealed how the presence of the Ir(III)-based complexes did not alter the morphology of colloidal silica and granulated phases. Moreover, the silica matrix did not interfere with the optical properties of the embedded complexes. The distribution of **[F_2IrPTZ-Me]$^+$** and **[IrQTZ-Me]$^+$** in the spray-freeze-dried powders was qualitatively evaluated by fluorescence microscopy, revealing how the luminescent particles were homogeneously dispersed all over the silica matrix. Interestingly, in aqueous solution the release of the complex **[F_2IrPTZ-Me]$^+$** from the corresponding **Ir@SiO_2 powder** is almost negligible, therefore suggesting the strong interaction occurring between the host-silica matrix and the Ir(III) guest complex.

Introduction

The scenario of iridium-transition metal complexes (Ir-TMCs) has been extensively expanded through a multitude of examples [1]. In this context, great efforts have been spent with the family of Ir(III) cyclometalates, a versatile class of compounds with general formula $[Ir(C^N)(N^N)]^{0/+}$ (C^N = phenylpyrdine - ppy - or 2, 4 difluoro-phenylpyrdine - F_2ppy-, N^N = diimine ligand, neutral or anionic) [2][3]. Taking advantage from their outstanding photophysical features - including a fine emission-colour tuning by ligand modification, long lived excited states (τ) and high quantum yield (Φ) values - Ir-TMCs can be considered as one of the most promising class of luminescent complexes [1]. In recent times, solid-state lightning (Organic Light Emitting Diode – OLEDs, Light Emitting Electrochemical Cells –LEECs [4]), heterogeneous catalysts [5] and luminescent bio-sensors [6] based on Ir-TMCs are in rapid development. This enhances the necessity of maintaining unaltered both chemical and photophysical stability of Ir(III) complexes at the experimental conditions that are required for their processing from liquid to solid-state (solvent, pH, temperature, etc.). This is a hard task to accomplish, because the optical properties Ir(III) complexes are detrimentally influenced by the interaction with surrounding environment that can alter the oxidation state of core metal, displace ligands form the complex, and promote the electron transfer towards surrounding species with expected quenching of luminescent outcomes. A potential solution to overcome this challenge is represented by the design of a stable anchoring platform capable of leaving unchanged the aforementioned properties [7]. Organic and bio-organic doped sol–gel materials have attracted much attention due to their ability to reproduce solution molecular activities within the ceramic environment. The processing versatility of the colloidal state permits the synthesis of multifunctional organic–inorganic hybrid structures through a bottom-up approach based on a tailored assembly of organic and inorganic building blocks [8]. In this regard, the use of silica nanoparticles (SiO_2NPs) as host-matrix for luminescent compounds has recently turned into a standard approach in the development of reliable sensors for various applications [9][10]. In addition to ready availability and low cost, SiO_2NPs also exhibit several fascinating properties, such as chemical, optical and thermal inertness together with high colloidal stability. The integration of metal complexes as active phase in SiO_2NPs host-matrix can accomplished by following different protocols, which include both chemical and physical methods [9][11]. In general, the chemical encapsulation of a guest molecule takes place during the formation of the silica solid phase (i.e. core-shell, Stöber method), while the physical approach (colloidal heterocoagulation, inorganic matrix encapsulation method) exploits the electrostatic

interactions between the negatively charged silica colloidal phase and the positively charged guest. The latter approach presents several advantages in comparison to core-shell protocols, since they don't require expensive reagents or chemical treatment, avoiding the formation of any byproduct. The main goal of the present study is to exploit and optimize new and easy to apply methods to incorporate Ir(III) tetrazolate complexes into silica-based colloid matrices, in order to improve their chemical and photophysical stability, enhancing their processing at liquid and dry state. Within this framework, two Ir(III) emitters bearing 5-aryl tetrazole ligands such as the sky-blue **$[F_2$IrPTZ-Me$]^+$** (C^N = F_2ppy; N^N = **PTZ-Me** - 2-(2-methyl-2*H*-tetrazol-5-yl)pyridine) and the red phosphorescent **[IrQTZ-Me]$^+$** (C^N = ppy; N^N = **QTZ-Me** -2-(2-methyl-2*H*-tetrazol-5-yl)quinoline) complexes (Scheme 1) were selected as cationic coatings for negatively charged SiO_2NPs, being able to cover the two opposite part of visible spectrum [12]. Prompted by the encouraging results in terms of both physical and optical stability, **Ir@SiO_2** nanosols were transferred to dry-powder state by the means of Spray-Freeze-Drying technique, an innovative procedure in the field that enabled the formation of two stable luminescent **Ir@SiO_2 powders** avoiding heat assisted drying processes that may alter both chemical and photophysical properties of the Ir(III) tetrazole complexes used as coating for silica nanoparticles [13][14][15].

Results and discussion

Synthesis of cationic Ir(III) tetrazolate complexes

The preparation of the cationic Ir(III) tetrazolate complexes **$[F_2$IrPTZ-Me$]^+$** and **[IrQTZ-Me]$^+$** was accomplished by following a previously reported procedure (Scheme 1) [12], which consists of an electrophilic addition at the tetrazole ring of the corresponding neutral Ir(III) precursor. The formation of the desired cationic Ir(III)-cyclometalates was at first confirmed by electrospray ionisation mass spectrometry (ESI-MS), which revealed the presence of the expected *m/z* signals in the positive region ions (Figure S5-6 ESI). The ^{1}H-NMR characterization provided a number of protonic resonances congruent with the low symmetry displayed by the complexes (Figure S1-2 ESI). As previously reported [12], the electrophilic addition performed on the $[R\text{-}CN_4]^-$ moiety regioselectively occurs at the N-2 atom of the tetrazolate ring, as witnessed by ^{13}C-NMR resonance of Ct (tetrazolic carbon) which has been found at 166.54 ppm for **$[F_2$IrPTZ-Me$]^+$** and 167.93 ppm for **[IrQTZ-Me]$^+$** (Figure S3-4 ESI).

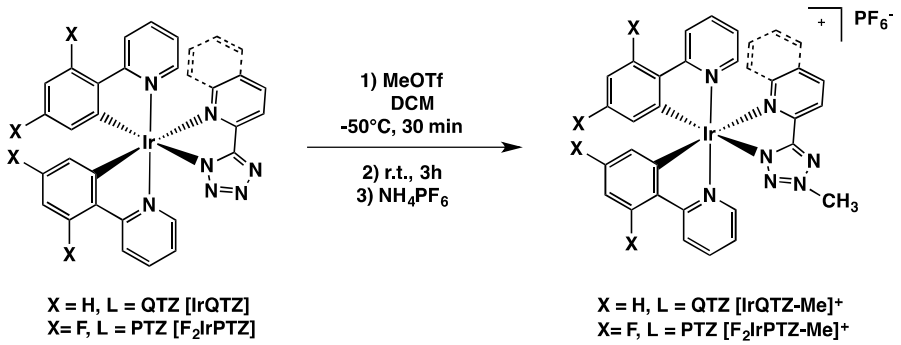

Scheme 1: Synthetic procedure used for cationic Ir(III) tetrazole complexes

Photophysical properties

In 10^{-5}M CH_2Cl_2 solutions, all the cationic Ir(III) complexes displayed similar absorption profiles, with intense ligand centred (^{1}LC) transitions up to 260 nm and metal-to-ligand charge transfer (^{1}MLCT) bands tailing off above 380 nm (Figure 1a).

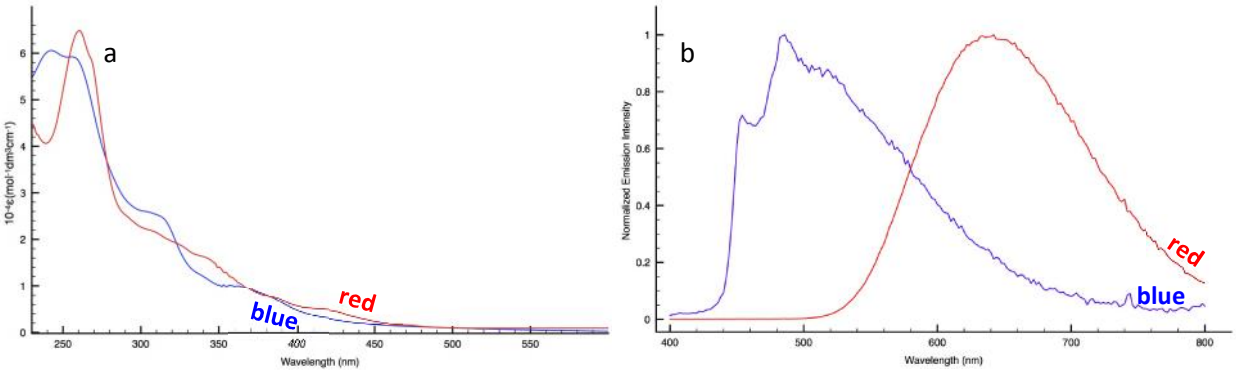

Figure 1: (a) Absorption Profiles of blue emitting **[F_2IrPTZ-Me]$^+$** (blue line) and red emitting **[IrQTZ-Me]$^+$** (red line), 10^{-5}M, CH_2Cl_2; (b) Normalized Emission Profiles of **[F_2IrPTZ-Me]$^+$** (blue line) and **[IrQTZ-Me]$^+$** (red line), CH_2Cl_2.

Upon excitation of the ^{1}MLCT features (λ = 370 nm), **[F_2IrPTZ-Me]$^+$** displayed a sky-blue emission colour that corresponds to a structured emission profile with λ_{max} = 454, 486 and 526 nm (Figure 1b and Table 1), suggesting an interplay of ^{3}LC/^{3}MLCT-type emissive excited states [1]. On the contrary, the red emitter **[IrQTZ-Me]$^+$** produced a broad and unstructured emission profile with λ_{max}= 638 nm, typical of ^{3}MLCT-based phosphorescence (Figure 1b), as evidenced also by the noticeable rigidochromic shift observed in frozen solvent matrix at 77K (λ_{max} = 568 nm, Table 1).

Table 1: Relevant absorption and emission data of cationic Ir(III) complexes discussed in this work.

CH_2Cl_2 as the solvent	**Absorption**	**Emission 298 K[a,b]**					**Emission 77K[c]**	
	λ_{abs}(nm);($10^{-4}\varepsilon$)($M^{-1}cm^{-1}$)	λ_{em} (nm)	τ_{air} (μs)	τ_{Ar} (μs)	ϕ_{air} (%)	ϕ_{Ar} (%)	λ_{em} (nm)	τ (μs)
[IrQTZ-Me]$^+$	253 (4.25), 310 (1.41), 374 (0.78)	638	0.220	0.550	2.8	4.5	568	1.56
[F_2IrPTZ-Me]$^+$	257 (6.24), 318 (2.70), 351 (1.20)	454, 486, 526	0.040	0.140	1.7	4.7	448, 480	6.62

[a]:"Air" means air equilibrated solutions, "Ar" means deoxygenated solutions under argon atmosphere; [b]: [Ru(bpy)$_3$]Cl$_2$/H$_2$O was used as reference for quantum yield determinations (Φ_r = 0.028); [c]: in frozen CH_2Cl_2

Ir@SiO_2 nanosols systems

Ir@SiO_2 nanosols (namely**: blue** Ir@SiO_2 for **[F_2IrPTZ-Me]$^+$** and **red** Ir@SiO_2 for **[IrQTZ-Me]$^+$**) were obtained by mixing the appropriate Ir(III) cationic complex with a silica suspension[16], which was previously destabilised through a cation-exchange resin treatment in which the replacement of Na^+ with H_3O^+ promotes the intra-particles cross-linking [17]. In this regard, an explanation is provided by Dumont and Watillon [18], that pointed out how the Na^+ substitution by H_3O^+ ions affects silica bonding, with the replacement of dissociated silanol-silanol bonds by cross-linked siloxane bonds: −Si−OH••••O^-−Si− ➔ −Si−O−Si + OH^-. In addition, the electrostatic stabilization of resin treated silica nanoparticles decreases; in fact, Zeta Potential passes from -42 to -29 mV as expected by the pH decrease from 9.0 to 4.5 (Table 2). The colloidal properties of **Ir@SiO_2 nanosols** systems were studied in respect of their hydrodynamic diameter and surface charge properties (Table 2). As evidenced by the Zeta Potential vs pH measurements (Figure 2), the presence of the phosphorescent Ir(III) tetrazole-markers did not affect the surface charge properties of SiO_2NPs. For all the silica colloidal solutions, the obtained plots revealed only one isoelectric point found at pH < 1.5, while the highest stability (ZP ≥ −30 mV) have been found between 3 < pH < 10 values. Furthermore, the hydrodynamic diameter of colloidal SiO_2NPs was not significantly affected by the physical mixing with the Ir(III)-markers, as confirmed by hydrodynamic radius (R_{hyd}) values obtained from DLS analyses (Table 2).

Table 2: Colloidal properties of silica based nanosols.

Sample	***pH***	***DLS R_{hyd} (nm)***	***Zeta Potential (mV)***
SiO_2_Ludox	9.0	20 ± 1	-42.2 ± 1.1
SiO_2*	4.5	23 ± 1	-29.0 ± 0.2
blue Ir@SiO_2	4.5	22 ± 2	-33.3 ± 1.8
red Ir@SiO_2	4.5	24 ± 1	-30.8 ± 1.5

**Commercial SiO_2 destabilized through treatment on cationic-exchange resin.*

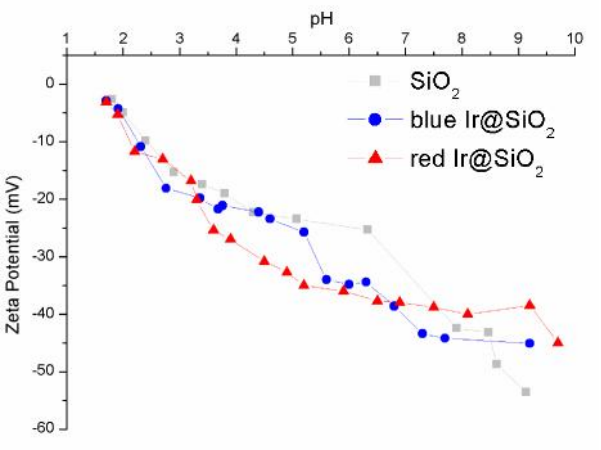

Figure 2: Zeta Potential (mV) vs pH plot of silica nanosol (grey line), blue Ir**@SiO₂** (blue line) and red Ir**@SiO₂** (red line), 100 mg/L of solid fraction.

The morphology of silica nanoparticles and the distribution of the Ir(III) complexes were examined by the means of TEM-EDX (Transmission Electron Microscopy-Energy Dispersive X-ray Analysis, Figure 3 and 4). The nanoparticles size distribution is homogeneously centered on 14 nm, being these values in accordance with the measured R_{hyd} (Table 2). TEM images highlight a negligible increase of the SiO_2 NPs mean diameter (ØSiO_2 13.7±3.1 nm, Ø **blue Ir@SiO₂** 13.8±3.1 nm, Ø **red Ir@SiO₂** 14.0±3.4 nm) and a slight improvement of particles cross-linking in the presence of complexes, forming necklace-like structures (Figure 3, B, C). TEM images acquired at higher magnification revealed the presence of a halo in the surroundings of SiO_2NPs, imputable to the presence of Ir(III) complexes, as shown in Figure 4 and confirmed by EDX analysis.

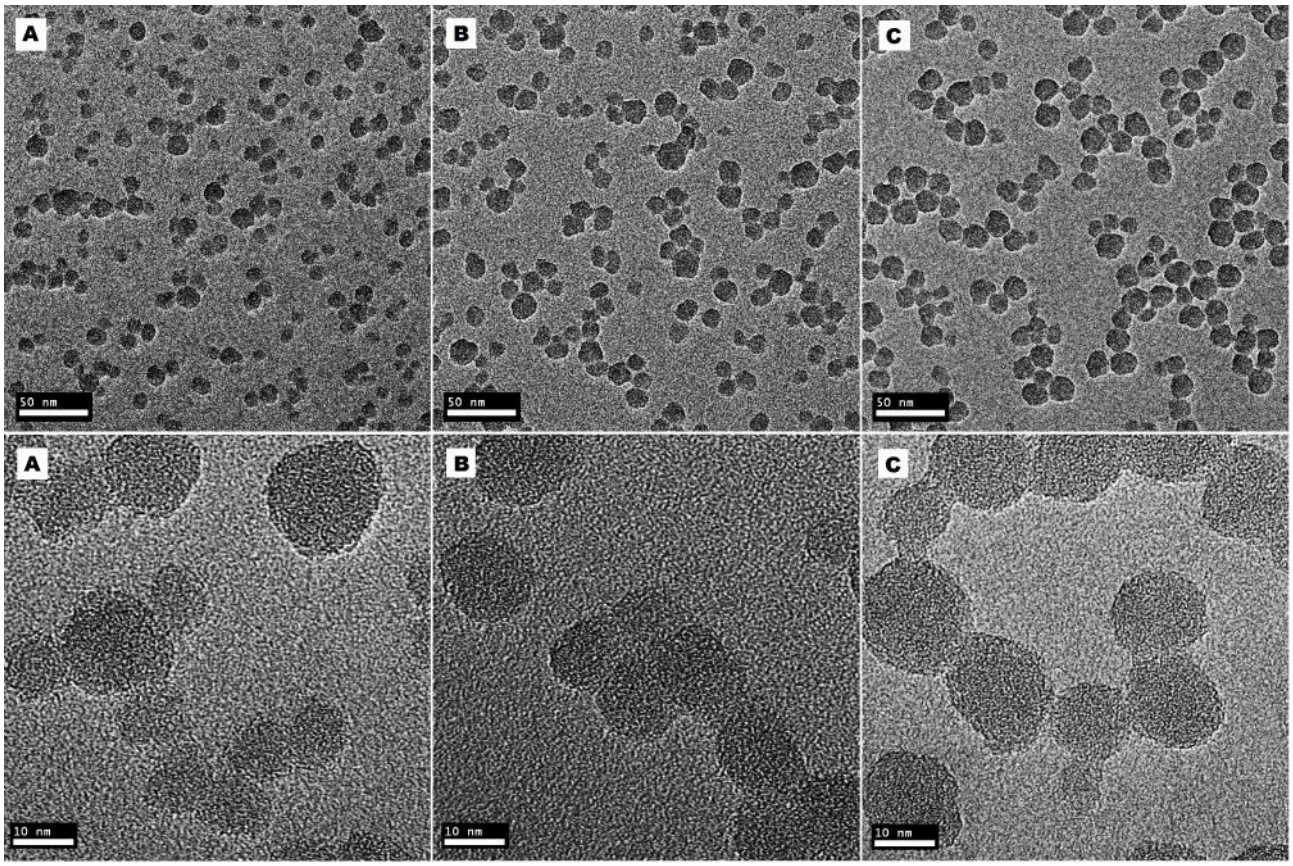

Figure 3: TEM images on copper grid acquired at different magnifications of A) SiO_2NPs, B) **blue Ir@SiO_2**, C) **red Ir@SiO_2**.

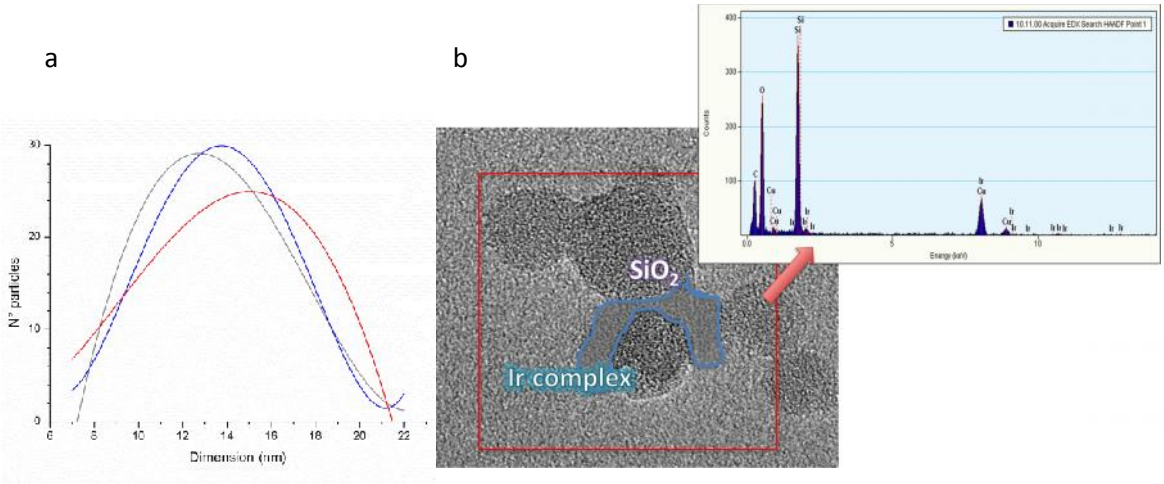

Figure 4: a) Nanoparticles distribution made by 250 particles-population: SiO_2NPs (grey line), **blue Ir@SiO_2** (blue line), **red Ir@SiO_2** (red line); b) TEM image of **blue Ir@SiO_2**, with relative EDS analysis.

As previously reported in literature [10], colloidal silica has no optical influence over the photoluminescent output of transition metal complexes, resulting transparent in both the

absorption (230-400 nm) and emission range (400-800 nm). This behavior was confirmed by the absorption profile of SiO_2NPs (Figure 5), where no maxima were found in the region of interest.

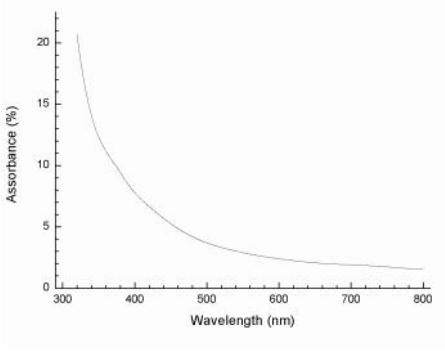

Figure 5: Absorbance (%) vs Wavelength (nm) plot of SiO_2NPs, 3%wt, Milli-Q H_2O, r.t.

Table 3: Relevant photophysical properties of Ir(III)-complexes@SiO_2 nanosols systems.

H_2O as solvent	***Absorption*** λ_{abs}(nm)	***Emission 298 K***				
		λ_{em} (nm)	τ_{air} (µs)	τ_{Ar} (µs)	φ_{air} (%)	$\Delta\lambda$ (nm)
Red Ir@SiO_2	252, 312	610	0.100	n.d.*	n.d.*	28
Blue Ir@SiO_2	263, 286, 310	454, 484, 520	0.010	n.d.*	n.d.*	0

**n.d. = not determined.*

The emission profiles of **[F_2IrPTZ-Me]$^+$** and its silica embedded structure **blue Ir@SiO_2** (Table 3 and Figure 6a) resulted almost superimposable to each other and did not provide any indication of the new chemical interaction established between **[F_2IrPTZ-Me]$^+$** and the silica matrix. On the other hand, the rigidochromic blue shift encountered in the emission profile of **red Ir@SiO_2** in respect of **[IrQTZ-Me]$^+$** (Table 3 and Figure 6b) is in agreement with the prevailing ^{3}MLCT composition of its excited state, being more sensitive to modifications of the surrounding chemical environment [1].

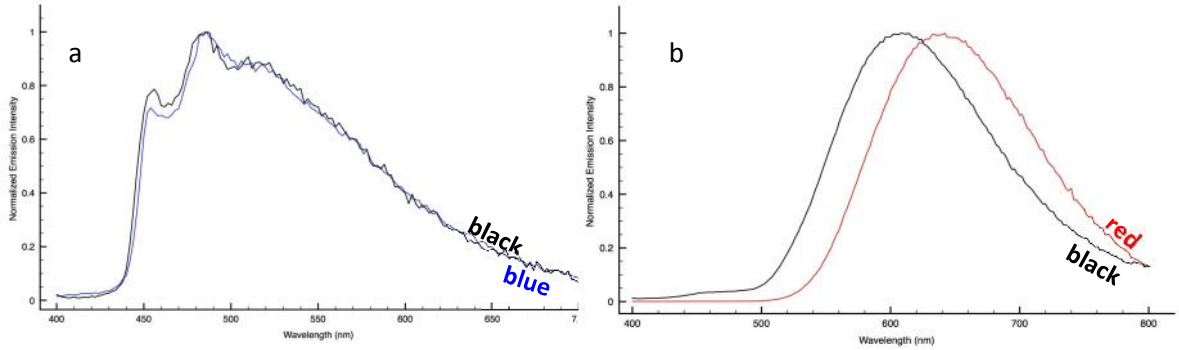

Figure 6: Comparison between normalised emission profiles **[F_2IrPTZ-Me]$^+$** (blue line) and **[IrQTZ-Me]$^+$** (red line) complexes and their **Ir@SiO_2 systems** (black lines).

Ir@SiO_2 powders

Both **blue** and **red Ir@SiO_2** nanosols were micronized and subsequently dried by the means of S*pray-Freeze-Drying* technique, an instantaneous process that, in comparison with heat promoted drying processes, is expected to maintain unaltered the photoluminescent properties of Ir@SiO_2 nanosols [11][19][20][21]. The morphology of the obtained **blue** and **red Ir@SiO_2 powders** was checked by optical microscopy and SEM-FEG. The microstructure of spray-freeze-dried granules of both SiO_2 and **Ir@SiO_2 powders** appeared spherical and regular, with a broad distribution (Figures 7 and 8). The mean diameter of **Ir@SiO_2 powders** was significantly reduced, from 22.6 ± 12.6 µm of SiO_2 considered alone to 17.5 ± 11.3 µm and 18.0 ± 11.4 µm for **Ir@SiO_2 powders**, as a result of an intense interaction between SiO_2NPs in the presence of phosphorescent complexes (Figure 9). The observed submicron homogeneously distributed porosity, shown in Figure 8, can be considered as induced by the sublimation of water from the silica colloidal solution, leaving a mesoporous structure. As a consequence, Specific Surface Area (SSA) measurements pointed out impressive values for both silica (207.78 ± 4.16 m^2/g) and Ir@SiO_2 powders (**blue Ir@SiO_2 powder**, 225.13 ± 4.50 m^2/g; **red Ir@SiO_2 powder**, 213.96 ± 4.28 m^2/g).

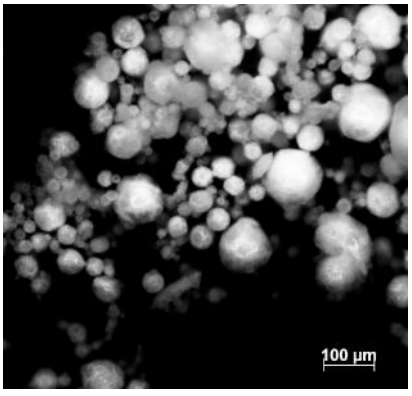

SiO_2-powder	**SEM-FEG granules-size (µm)**
blue Ir@SiO_2 powder	17.5 ± 11.3 µm
red Ir@SiO_2 powder	18.0 ± 11.4 µm
SiO_2	22.6 ± 12.6 µm

Figure 7: Optical micrograph of **SiO_2 powder**.

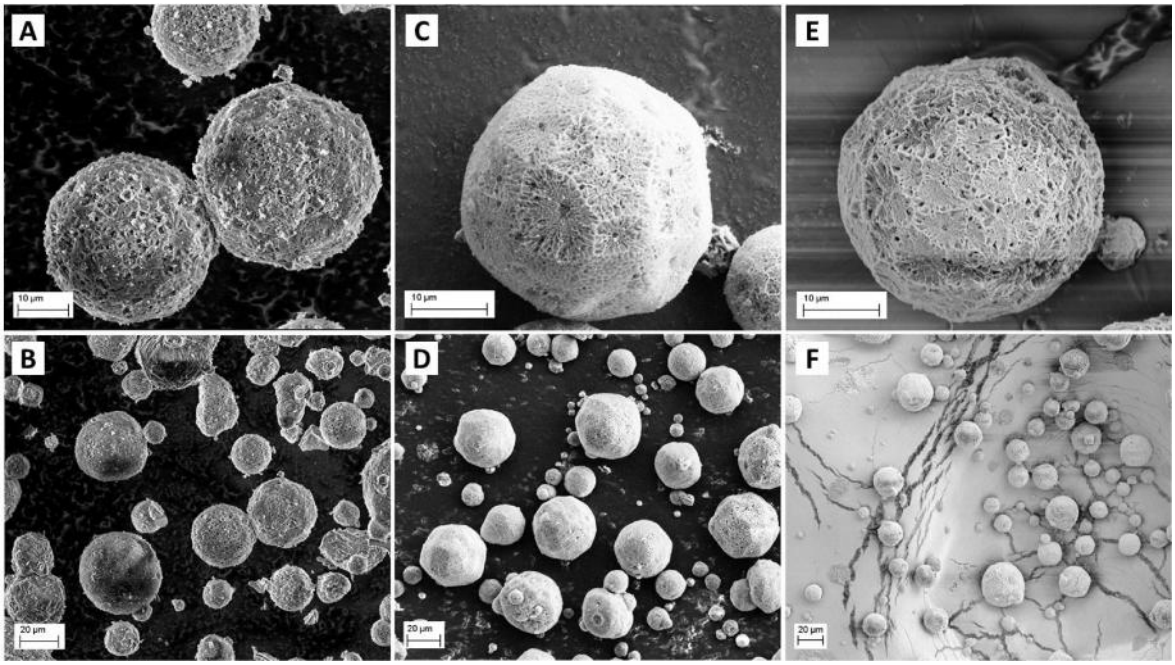

Figure 8: SEM-FEG images of SiO_2 (A, B), **blue Ir@SiO_2 powder** (C, D) and **red Ir@SiO_2 powder** (E, F).

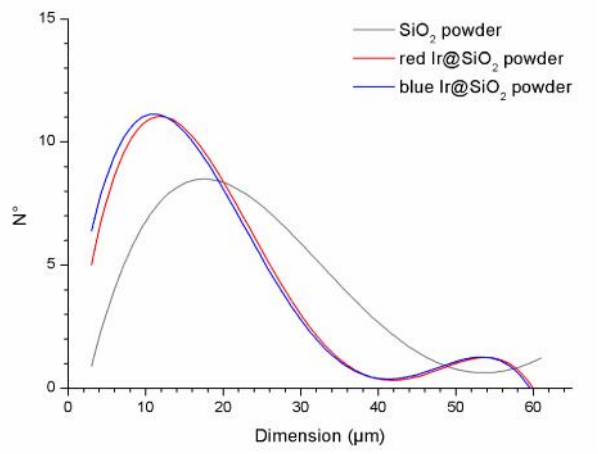

Figure 9: Size distribution of micronized SiO_2 powders (grey trace), **blue Ir@SiO_2 powder** (blue trace) and **red Ir@SiO_2 powder** (red trace). The mean value was calculated for a population of 250 particles.

As previously discussed for Ir@SiO_2 nanosols, only the **red Ir@SiO_2 powder** (λ_{max}=577 nm) displayed a significant rigidochromic blue shift in comparison to **[IrQTZ-Me]$^+$** (Figure 10). This behavior was further confirmed by variable temperature emission studies over the range 15-300K, where no substantial changes were observed for the **blue Ir@SiO_2 powder** (Figure 11a), while for the **red** one, a blue shift of the emission maxima from to 570 to 550 nm was detected (Figure 11b) [1]. In both cases, the presence of surrounding silica matrix and the temperature decrease are two driving forces that change the environment polarity, stiffening the system structure and modulating the final phosphorescent outcome of the **red Ir@SiO_2 powder**.

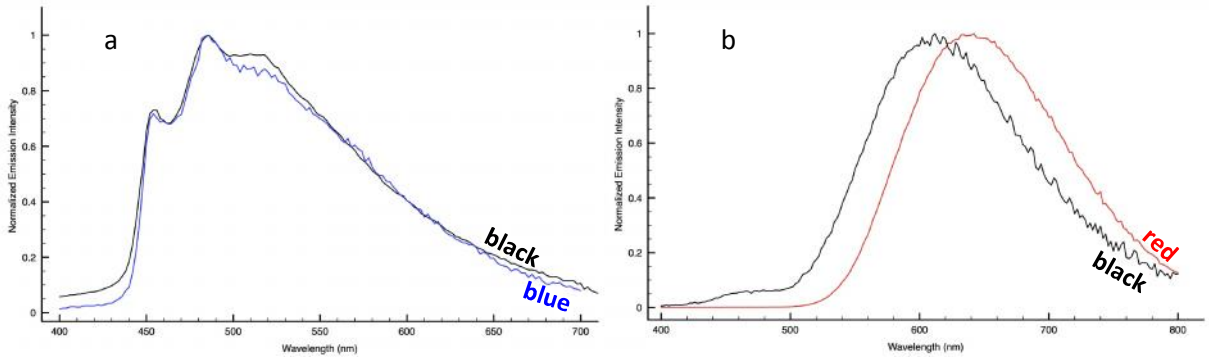

Figure 10: a) Normalized Emission Profiles of **[F_2IrPTZ-Me]$^+$** (blue line) and **blue Ir@SiO_2 powder** (black line); b) Normalized Emission Profiles of **[IrQTZ-Me]$^+$** (red line) and **red Ir@SiO_2 powder** (black line).

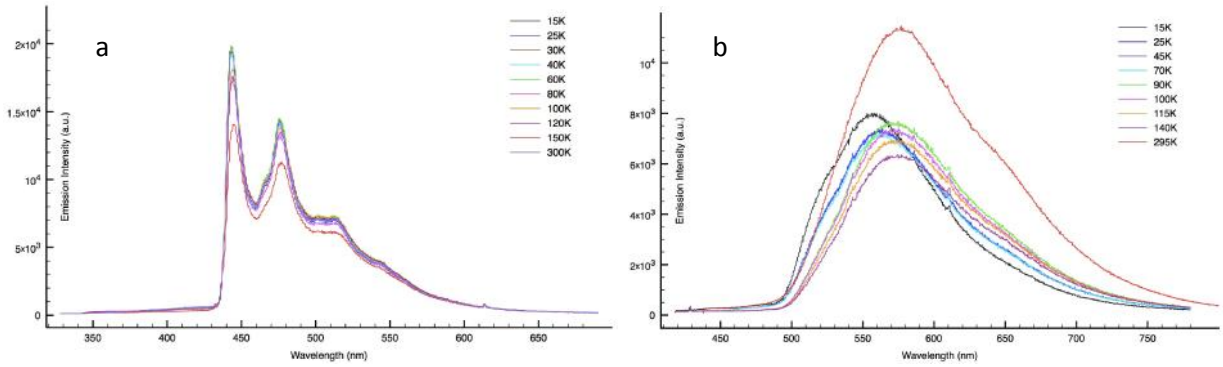

Figure 11: Variable temperature emission studies of a) **blue Ir@SiO_2 powder** and b) **red Ir@SiO_2 powder** (15-300 K).

The distribution of **[F_2IrPTZ-Me]$^+$** and **[IrQTZ-Me]$^+$** complexes in the ceramic micronized powders were evaluated by fluorescence microscopy (Figure 12). For both **Ir@SiO_2 powders**, the luminescent properties resulted homogeneously spread over the silica matrix. Using *Spray-Freeze-Drying* technique, we avoided any possible thermal degradation, as that a Spray-Drying processes can induce with a consequent damage or deface of Ir(III) complexes luminescent properties. The Ir@SiO_2 nanosol were sprayed and frozen, thus preserving the NPs and complexes distribution as was in dispersed liquid phase. No separate cluster of luminescent marker are appreciated and a distribution of spherical luminescent micro-particles was detectable under fluorescence microscope.

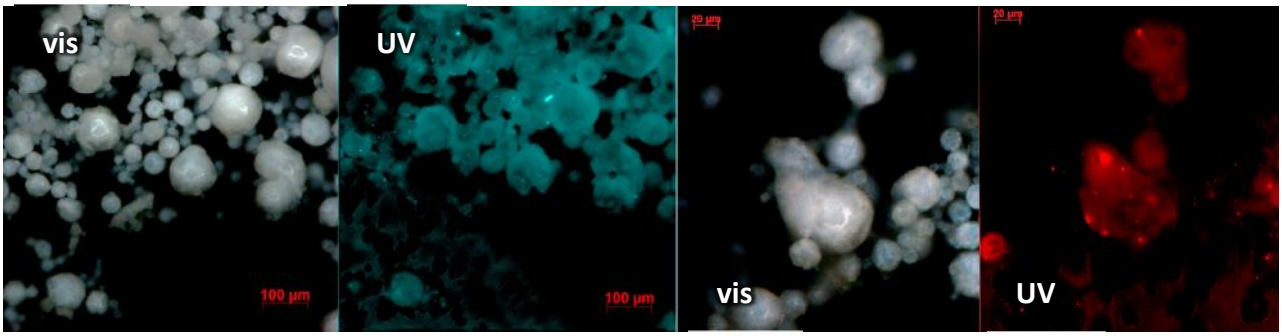

Figure 12: Micrographs of (left) **blue Ir@SiO_2 powder** and (right) **red Ir@SiO_2 powder** with visible and fluorescence source.

The wettability of **Ir@SiO_2 powders** was evaluated by observing the particles morphology in the presence of water ("Drop-Test", Figure 13). **Ir@SiO_2 powders** preserved their spherical shape without decomposing in a time period of 15 minutes, thus exhibiting some mechanical strength even after water-contact, encouraging the use of these systems in the large spectrum of wet powder process applications.

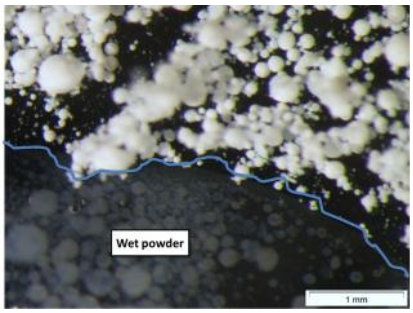

Figure 13: Drop-test for **blue Ir@SiO_2 powder** acquired with OLYMPUS SZX9.

The release of **[F_2IrPTZ-Me]$^+$** from the **blue Ir@SiO_2 powder** was evaluated in both organic and inorganic media (CH_3CN, CH_2Cl_2 and H_2O; see Figure 12 and S7-8 ESI), by acquiring emission spectra of the liquid phase separated from the suspension of **blue Ir@SiO_2 powder,** kept under mechanical stirring for approx. 25 hours (Figure 14). The emission profiles suggest a very low release percentage of **[F_2IrPTZ-Me]$^+$** (presumably below 10^{-9} M), confirming the strong interaction occurring between the host-silica matrix and the **[F_2IrPTZ-Me]$^+$** complex.

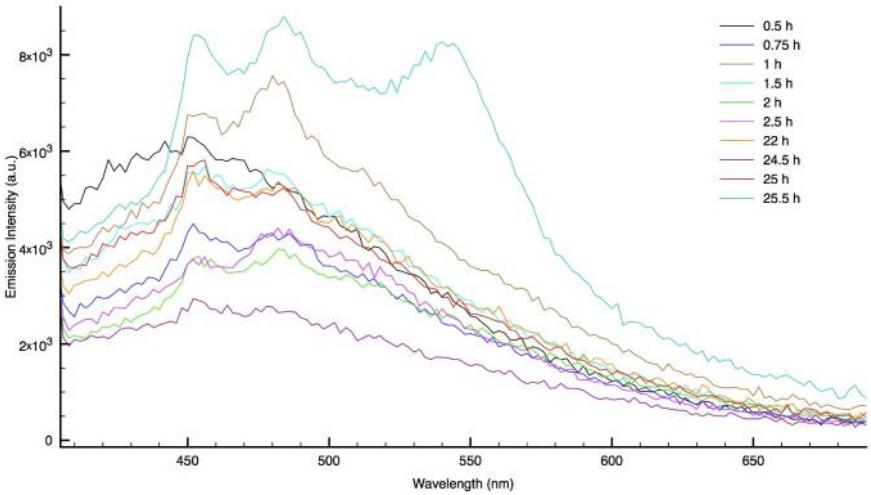

Figure 14: Water-release emission test of **[F_2IrPTZ-Me]$^+$** from **blue Ir@SiO_2 powder**.

Conclusions

In summary, we have demonstrated how **[F_2IrPTZ-Me]$^+$** and **[IrQTZ-Me]$^+$** tetrazole complexes can be successfully incorporated into a silica matrix, with a simple and easily scalable colloidal route. We design a multi-scale process, and obtained luminescent powders that preserved optical properties from molecular scale to micro scale, providing a self-marking ceramic platform stable and easy to be processed at dry or wet dispersed state. The silica embedded Ir(III) complexes could be effectively isolated and sterically confined within micro granules obtained by spray-freeze-drying the correspondent nanosol. The luminescent properties stemming from **[F_2IrPTZ-Me]$^+$** and **[IrQTZ-Me]$^+$** resulted homogeneously spread over the silica matrix, as confirmed by fluorescence microscopy. The granulated Ir@SiO_2 powders preserved their spherical shape without decomposing in water and did not release free complex neither in contact with aqueous nor with organic solvents. We confirmed the photostability of Ir@SiO_2 systems by comparing the luminescent properties of the complexes themself and in the presence of silica host matrix, either as sol or in the solid state. Finally, the great versatility of cationic Iridium(III) tetrazole complexes, compared to other classes of organometallic complexes, makes room for further investigations, with the aim to cover all visible spectrum. In fact, we are able to obtain different emission, by changing ligands, that are modulated by encapsulation but a stable silica matrix. These encouraging results pave the way for the employment of these phosphorescent powders in various fields, ranging from nanoengineering materials (LED colour converter, photonics, optoelectronics, photo-induced catalysis or industrial anti-counterfeiting) to nanobiotechnology

(imaging, targeting, and sensing), where long-term stability with high luminescent efficiency is required.

Experimental Section

General Considerations. All the reagents and solvents were obtained commercially (e.g. Merck, Alfa Aesar, Strem Chemicals) and used as received without any further purification. The commercial colloidal suspension of silica (Silica LUDOX® HS-40) was supplied by Grace Davison and destabilized using a commercial exchange resin Dowex 50x8 protons (Merck), with MESH value of 20-50 and total exchange capacity of 1.7 meq/mL. The purification of the Ir(III) complexes was performed via column chromatography with the use of Al_2O_3 as the stationary phase. ESI-mass spectra were recorded using a Waters ZQ-4000 instrument (ESI-MS, acetonitrile as the solvent). Nuclear magnetic resonance spectra (consisting of ^{1}H and ^{13}C) were always recorded using a Varian Mercury Plus 400 (^{1}H, 399.9; ^{13}C, 101.0 MHz). ^{1}H and ^{13}C chemical shifts were referenced to residual solvent resonances.

Ligand synthesis. Warning! Tetrazole derivatives are used as components for explosive mixtures[22]. In this lab, the reactions described here were only run on a few grams scale and no problems were encountered. However, great caution should be exercised when handling or heating compounds of this type. Following the general method reported by Koguro and co-workers[23], tetrazole ligands [H-**PTZ**] and [H-**QTZ**] has been obtained in quantitative yield.

General Procedure for the Preparation of the Cationic Ir(III) complexes. The preparation of cationic Ir(III)-complexes was accomplished by following a previously reported procedure [12]. 1 eq of the desired neutral Ir(III) tetrazolate complex was added to dichloromethane and the mixture was allowed to cool down by immersion into an ethanol/liquid nitrogen cold bath. Then, methyl trifluoromethanesulfonate (1.2 equiv., solution in dichloromethane 0.179 M) was added. The reaction was stirred under nitrogen for 30 minutes while being kept in the cold bath, and then allowed to warm up to room temperature and stirred for 3 hours. Anion exchange was carried out by adding an excess of NH_4PF_6 in water to the solution and stirring for 20 minutes. The product was then extracted using dichloromethane (3×10 mL) and the organic components were combined and dried over anhydrous $MgSO_4$. Subsequent purification by column chromatography on alumina (gradient: CH_2Cl_2/acetone 8:2, second fraction) yielded 0.059 g of **$[F_2$IrPTZ-Me$]^+[PF_6]^-$** and 0.067 g of **$[$IrQTZ-Me$]^+[PF_6]^-$**.

General procedure for the colloidal physical encapsulation. The Ir(III)-tetrazole based nanosols were produced by mixing $[F_2IrPTZ\text{-}Me]^+$ or $[IrQTZ\text{-}Me]^+$ with Silica LUDOX® HS-40 destabilized using Dowex 50x8 protons, a commercial exchange resin (Ir(III)tetrazole complex : SiO_2 nanosol ratio = 1:1000, w silica (%) = 20). To facilitate the mixing and the intimate interaction between the two phases, the systems were left under stirring for about 24 hours at ball-milling, in presence of grinding bodies made by zirconia balls (diameter, Ø 5mm). The Silica LUDOX® HS-40 destabilization was carried out in a 250 mL flask by adding the resin to the nano-suspension under vigorous stirring. Once the desired pH was reached (pH = 4), the resin was extracted and the silica/resin contact was interrupted by vacuum pump filtration [17].

General procedure for the Solid-state transfer by Spray Freeze Granulation. The silica-doped colloidal solutions were transferred to solid-state phases by the means of Lab-scale Granulator LS-2 (PowderPro AB). The two Ir(III)@SiO_2 nanosol were kept under magnetic stirring to prevent solid sedimentation and fed to the nozzle (Ø = 100 μm) through a peristaltic pump (40 rpm). The spray was obtained by blowing suspension and nitrogen (0.4 bar) in the nozzle, collecting the nanosol drops in a camera that was previously filled up with liquid nitrogen. The frozen drops were placed in a metallic vessel inside the lyophilizer for 4 days, reaching the pressure of 1.5 mbar.

Colloidal Characterization. Size and ZP (Zeta Potential) measurements of the nano-solutions were carried out with DLS/ELS (dynamic light scattering and electrophoretic light scattering Zetasizer Nano instrument ZSP, ZEN5600, Malvern Instruments, UK). The study of the colloidal behaviour and the interaction between silica and Ir(III) complexes (Zeta potential vs pH) were carried out by Zetasizer Nano instrument coupled with an automatic titrating system. The titration were performed with 1M KOH and 1M HCl solutions on Ir(III)@SiO_2 systems at a concentration of 0.01%wt. The interaction between Ir(III) complexes and silica nanosol matrix was evaluated with TEM (transmission electron microscopy, FEI, Tecnai F20 S/TEM) equipped with an EDX probe.

Morphological Powder Characterization. The morphological characterization of freeze-dry particles was performed by SEM-FEG electron emission scanning microscope (Supra, Gemini Column, Zeiss) and by Optical Stereo Microscope OLYMPUS SZX9 with Nikon DS-Fi2 camera and ocular OLYMPUS DF PL 2xa (OLYMPUS).

Optical Powders Characterization. To estimate the optical inactivity of SiO_2 in respect of Ir(III)-complexes, the 3%wt silica LUDOX® HS-40 nanosol have been analyzed at spectrophotometer Lambda 35 (Perkin Elmer). The degree of dispersion of the Ir(III) complexes within the silica matrix was checked by optical microscope Zeiss, AXIO Zoom V16 equipped with CL 9000 LED white source (900 lm, 6500K, emission spectrum 400-800nm), while for luminescence microscopy images with a HXP 120V source metal halide lamp (emission spectrum 360-670 nm, excitation filter: BP = 470 ± 40 nm, beam splitter: FT = 495 nm, emission: BP = 525 ± 50 nm).

Photophysical characterization. Absorption spectra were recorded at room temperature using a Perkin Elmer Lambda 35 UV/vis spectrometer. Uncorrected steady-state emission and excitation spectra were recorded on an Edinburgh FLSP920 spectrometer equipped with a 450 W xenon arc lamp, double excitation and single emission monochromators, and a Peltier-cooled Hamamatsu R928P photomultiplier tube (185−850 nm). Emission and excitation spectra were acquired with cut-off filter (395 nm) and corrected for source intensity (lamp and grating) and emission spectral response (detector and grating) by a calibration curve supplied with the instrument. The wavelengths for the emission and excitation spectra were determined using the absorption maxima of the MLCT transition bands (emission spectra) and at the maxima of the emission bands (excitation spectra). Quantum yields (Φ) were determined using the optically dilute method by Crosby and Demas [24] at excitation wavelength obtained from absorption spectra on a wavelength scale [nm] and compared to the reference emitter by the following equation:

$$\phi_s = \phi_r \left[\frac{A_r(\lambda_r)}{A_s(\lambda_s)}\right]\left[\frac{I_r(\lambda_r)}{I_s(\lambda_s)}\right]\left[\frac{n_s^2}{n_r^2}\right]\left[\frac{D_s}{D_r}\right]$$

where A is the absorbance at the excitation wavelength (λ), I is the intensity of the excitation light at the excitation wavelength (λ), n is the refractive index of the solvent, D is the integrated intensity of the luminescence, and Φ is the quantum yield. The subscripts r and s refer to the reference and the sample, respectively. A stock solution with an absorbance > 0.1 was prepared, then two dilutions were obtained with dilution factors of 20 and 10, resulting in absorbance of about 0.02 and 0.08 respectively. The Lambert-Beer law was assumed to remain linear at the concentrations of the solutions. The degassed measurements were obtained after the solutions were bubbled for 10 minutes under Ar atmosphere, using a septa-sealed quartz cell. Air-equilibrated $[Ru(bpy)_3]Cl_2/H_2O$ solution (Φ = 0.028) [25] was used as reference. The quantum yield

377 determinations were performed at identical excitation wavelengths for the sample and the
378 reference, therefore deleting the I(λr)/I(λs) term in the equation. Emission lifetimes (τ) were
379 determined with the single photon counting technique (TCSPC) with the same Edinburgh FLSP920
380 spectrometer using pulsed picosecond LED (EPLED 360, FWHM < 800ps) as the excitation source,
381 with repetition rates between 1 kHz and 1 MHz, and the above-mentioned R928P PMT as
382 detector. The goodness of fit was assessed by minimizing the reduced χ2 function and by visual
383 inspection of the weighted residuals. To record the 77 K luminescence spectra, the samples were
384 put in quartz tubes (2 mm diameter) and inserted in a special quartz Dewar filled with liquid
385 nitrogen. The solvent used in the preparation of the solutions for the photophysical investigations
386 was of spectrometric grade. Experimental uncertainties are estimated to be ±8% for lifetime
387 determinations, ±20% for quantum yields, and ±2 nm and ±5 nm for absorption and emission
388 peaks, respectively. The pellets used in the variable-temperature emission experiments have been
389 obtained by using 50 mg of **$[F_2IrPTZ\text{-}Me]^+@SiO_2$ powder** or **$[IrQTZ\text{-}Me]^+@SiO_2$ powder** squashed
390 in a cylinder-shaped metallic tube (Ø 0.5 cm) for 1 min under 1 ton. The variable-temperature
391 emission spectra (from 13K to r.t.) were recorded with an SP500i Spectrometer (ACTION
392 RESEARCH, grating 150gr/mm, slit 50 µm) equipped with a sensitive liquid nitrogen-cooled CCD
393 camera and a He-Cd laser (KIMMON company) at 325 nm as excitation source (spot size = 100 µm,
394 power = 30mW).

395 *BET analysis.* The Specific Surface Area (SSA) measurements were carried out with a Surfer
396 instrumentation (Thermo Scientific) (P= 150–300 torr, T= -200°C). Before performing analysis, the
397 samples were thermal pre-treated (120°C) to eliminate any organic traces.

398 *Micronized Stability***.** The stability of micronized powders has been evaluated through time-release
399 tests under mechanical stirring. A 0.1 g amount of Ir(III)@SiO_2 nano-powder and 10 mL of Milli-Q
400 H_2O were stirred for different contact time (from 30 min to 25.5 h). After each period, 0.5 mL of
401 the suspension were removed and added to 5 mL of fresh Milli-Q H_2O and subsequently analyzed.

402 **Acknowledgement**

403 This project has benefited from the EU-H2020 research and program under grant agreement N°
404 654360 having benefitted from the access provided by Fundacio Institut Català de Nanociència y
405 Nanotecnologia - ICN2 - Barcelona (Spain) and Foundation for Research and Technology Hellas –
406 FORTH - Heraklion (Greece) within the framework of the NFFA-Europe Transnational Access
407 Activity. The ICN2 is funded by the CERCA programme (Generalitat de Catalunya) is supported by

the Severo Ochoa programme of the Spanish Ministry of Economy, Industry and Competitiveness (MINECO, grant N° SEV-2013-0295). The authors wish to thank the Italian Ministry of Education, University and Research (MIUR) for financial support (PRIN project: Towards a Sustainable Chemistry: Design of Innovative Metal–Ligand Systems for Catalysis and Energy Applications).

Graphical Abstract

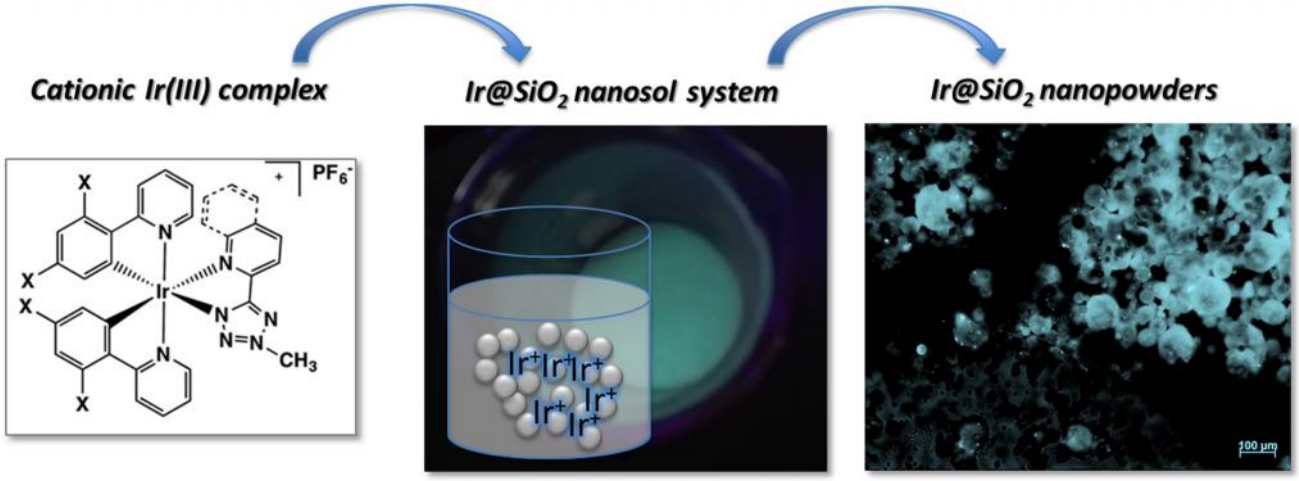

References

[1] L. Flamigni, A. Barbieri, C. Sabatini, B. Ventura and F. Barigelletti, *Top. Curr. Chem.*, 2007, **281**, 143–203.

[2] S. Stagni, S. Colella, A. Palazzi, G. Valenti, S. Zacchini, F. Paolucci, M. Marcaccio, R. Q. Albuqerque and L. De Cola, *Inorg. Chem.*, 2008, **47**, 10509–10521.

[3] V. Fiorini, S. Zacchini, P. Raiteri, R. Mazzoni, V. Zanotti, M. Massi and S. Stagni, *Dalton Trans.*, 2016, **45**, 12884-12896.

[4] H. Xu, R. Chen, Q. Sun, W. Lai, Q. Su, W. Huang and X. Lui, *Chem. Soc. Rev.,* 2014, **43,** 3259–3302.

[5] S. Takizawa, R. Aboshi and S. Murata, *Photochem. Photobiol. Sci.*, 2011, **10**, 895.

[6] a) V. Fernandez-Moreira, F. L. Thorp-Greenwood and M. P. Coogan, *Chem. Commun*., 2010, **46**, 186–202; b) K. Y. Zhang and K. K.-W. Lo, Chemosensing and Diagnostics, in Coordination and Organometallic Chemistry (Volume 8) of Comprehensive Inorganic Chemistry II, ed. V. W.-W. Yam, Elsevier, Amsterdam, 2013, pp. 657–732 and references cited therein.

[7] W. Liang, Y. Zhuo, C. Xiong, Y. Zheng, Y. Chai and R. Yuan, *Biosens. Bioelectron.,* 2017, **94**, 568–574.

[8] G. Kickelbick, Introduction to Hybrid Materials, in Hybrid Materials: Synthesis, Characterization, and Applications Wiley-VCH Verlag GmbH & Co. KGaA, Weinheim, Germany. doi: 10.1002/9783527610495.

[9] S. Titos-Padilla, E. Colacio, S. J. A. Pope, J. J. Delgado, M. Melgosa and J. M. Herrera, *J. Mater. Chem. C*, 2013, **1**, 3808.

[10] S. Santra, P. Zhang, K. Wang, R. Tapec and W. Tan, *Anal. Chem.,* 2001, **73**, 4988–4993.

[11] D. Gardini, M. Blosi, C. Delpivo, S. Ortelli and A. L. Costa, *J. Phys. Conf. Ser.,* 2013, **429**, 12052.

[12] V. Fiorini, I. Zanoni, S. Zacchini, A. L. Costa, A. Hochkoeppler, V. Zanotti, A. M. Ranieri, M. Massi, A. Stefan and S. Stagni, *Dalt. Trans.*, 2017, **46**, 12328.

[13] M.E. Ali, A. Lamprecht, Spray freeze drying for dry powder inhalation of nanoparticles, Eur. J. Pharm. Biopharm. 87 (2014) 510–517.

[14] A. L. Costa, B. Ballarin, A. Spegni, F. Casoli and D. Gardini, *J. Colloid Interface Sci.*, 2012, **388**, 31–39.

[15] C. Anandharamakrishnan, Spray Drying; Freeze Drying; Spray Freeze Drying. in *Handbook of Drying for Dairy Products,* 2017*,* 57–148.

[16] G. Davison, Q. Grace, Sílice coloidal ludox ® hs-40.

[17] S. Ortelli, A. L. Costa and M. Dondi, *Materials (Basel).,* 2015, **8**, 7988–7996.

[18] F. Dumont, and A. Watillon, *Discuss. Faraday Soc.,* 1971, **52**, 352–360.

[19] Y -F. Maa, P -A. Nguyen, T. Sweeney, S. J. Shire and C. C. Hsu, *Pharm. Res.,* 1999, **16**, 249–254.

[20] L. F. Ballesteros, M. J. Ramirez, C. E. Orrego, J. A. Teixeira and S. I. Mussatto, *Food Chem.,* 2017, **237**, 623–631.

[21] L. Alamilla-Beltrána, J. J. Chanona-Péreza and A. R. Jiménez-Apariciob, *J. Food Eng.,* 2005, **67**, 179–184.

[22] Butler, R. N. Tetrazoles. In 'Comprehensive Heterocyclic Chemistry II'; Storr, R. C., Ed.; Pergamon Press: Oxford, U.K., 1996, Vol. 4, 621-678, and references cited therein.

[23] K. Koguro, T. Oga, S. Mitsui, and R. Orita, *Synthesis,* 1998, 910–914.

[24] G. A. Crosby and J. N. Demas, *J. Phys. Chem.*, 1971, **75,** 991–1024.

[25] K. Nakamura, *Bull. Chem. Soc. Jpn*., 1982, **55**, 2697–2705.